Progress In Electromagnetics Research B, Vol. 63, 187–201, 2015

Analysis of the Proximity Coupling of a Planar Array Quasi-Lumped Element Resonator Antenna Based on Four Excitation Sources

Seyi S. Olokede[1, *] and Clement A. Adamariko[2]

Abstract—In this paper, a simple-fed, low profile, 9×10 elements quasi-lumped planar antenna array is presented. The proposed resonator employs a quasi-lumped element resonator that uses interdigital capacitor (IDC) in parallel with a straight strip inductor shorted across the capacitor. The array elements were designed and then excited by a feed network of four coaxial probes situated at the bottom plane but separated from the ground plane using a plastic material. The entire array is divided into four sub-array lattices of 5×5 elements and excited by a coaxial probe located at the centre of the sub-arrays antenna structure, thus exciting the centre resonator who in turn excites the neighbouring elements via proximity coupling. The probes are connected based on Wilkinson power divider principle to provide in-phase excitation. An explicit method is introduced to quickly obtain the array factor (AF) characteristics for such proximity coupled rectangular planar array. Radiation pattern and the array factor are presented, and are further compared with those obtained by the simulation and experimental results. The proposed antenna comprises 9×10 elements array, each of which is 5.8×5.6 sq. mm in size, and the entire antenna structure is about 120×80 sq. mm.

1. INTRODUCTION

Usually, lumped element resonators are formed by lumped inductors and capacitors. These lumped element resonators are passive components whose sizes across any dimension are much smaller than the operating wavelength to ensure that there is no appreciable phase shift between the input and output terminals. Their no-phase shift tendency underscores their usefulness. As a result, most literatures recommend that the length of an equivalent inductor and capacitor elements should not be longer than $\lambda/20$ or 12% of its wavelength of operation. Otherwise, it will lose its lumped equivalency effect. However, Janhsen et al. [1] asserted that a general definition of quasi lumped elements cannot be established particularly with reference to its length, because it would be somewhat arbitrary. Incidentally (according to them), the width w of an impedance sections has only a small effect on the scattering parameters in comparison with the length l, where the height h of the sections is oriented transversely to the current flow. Of particular interest therefore is the definition of Hong where he defined quasi-lumped element as microstrip line short sections and stubs whose physical lengths are smaller than a quarter of guided wavelength at which they operate, and as such, are common components for approximate microwave realization of lumped elements in microstrip filters structures, and are termed quasi-lumped elements [2]. It is on the basis of this definition that the proposed derives its lumped element equivalency. They therefore have the relative advantage of smaller size, wider bandwidth, and more particularly, lower cost characteristics. Thus, impedance transformation close to 20:1 is feasible using quasi-lumped element resonator [1].

Received 27 February 2015, Accepted 2 September 2015, Scheduled 18 September 2015
* Corresponding author: Seyi Stephen Olokede (solokede@gmail.com).
[1] School of Electrical & Electronic Engineering, Universiti Sains Malaysia, Nibong Tebal 14300, Malaysia. [2] Department of Electrical Engineering, University of Ilorin, PMB 1515, Ilorin, Kwara State, Nigeria.

Analysis of linear and planar arrays either for large or compact antennas, including dipole antenna, monopole antenna, and planar antenna configurations, have been extensively studied and well reported in some publications. These works, though efficient suffer significant large antenna size. However, in [2], the authors reported the design of an efficient miniaturized UHF planar antenna employing spiral slot radiating elements. This work is noteworthy and adequate for UHF applications but suffer serious disadvantage most especially at high frequencies range of applications as it becomes unrealizable due to etching limitations. This paper therefore presents an efficient compact planar array quasi-lumped element resonator antenna for WLAN applications. The objectives of this paper in the first instance is to present the single quasi-lumped element resonator's performance profile with the view to determining its compactness; the second is to derive the requisite surface current density equations of the proposed resonator bearing in mind the edge and boundary condition singularity requirement; the third is to investigate the proximity coupling between the radiating elements, and much more to derive explicit formulae for the coupling and array factor (AF) using a numerical method; the fourth objective is to design the proposed planar array configuration having proved that the single quasi-lumped element resonator footprint is compact and efficient, in order to provide requisite platform to further validate the derived explicit numerical formulae; and finally, design a conventional microstrip patch planar array for performance profile comparison with the proposed antenna so as to demonstrate its specific advantages. To this effect, the proposed antenna becomes attractive for wireless communication applications.

2. THEORETICAL BACKGROUND

2.1. Single Quasi-Lumped Element Resonator Antenna

The single quasi-lumped element resonator consists of quasi-lumped microstrip line sections and stubs, which employs an interdigital finger capacitor (IDC) in parallel with a single narrow straight conductor. A meander-line inductor may also be used alternatively to improve the capacitance. The inductor (L) is the centre finger shorted across the capacitor. The pads connected at both ends of the structure act as capacitors to ground (C_P), which can be adjusted to tune the resonant frequency of the resonator. The layout of the quasi-lumped element resonator and equivalent circuit of the structure are shown in Figure 1(a). The capacitor C is an interdigital capacitor (IDC), an inductor L is the microstrip inductor whereas capacitor C_{p1} and C_{p2} are pad capacitances. The interdigital capacitor C is a comb-like, digit-like or finger-like periodic pattern deposited on a broad types of substrates which could be porous, transparent or opaque [3]. In order to create high-Q (a figure of merit, which is a measure of the performance or quality of a resonator) a planar IDC is deposited on the surface of a relatively high dielectric constant substrate. The Q-factor can be enhanced by using high-conductivity conductors, low-loss tangent dielectric materials, Q-enhancement techniques including suspended substrate, multilayer structures and macro-machining [4]. The essence of IDC is to build up the capacitance associated with the electric field that penetrates into the substrate. Generally, it relies on the strip-to-strip (gap)

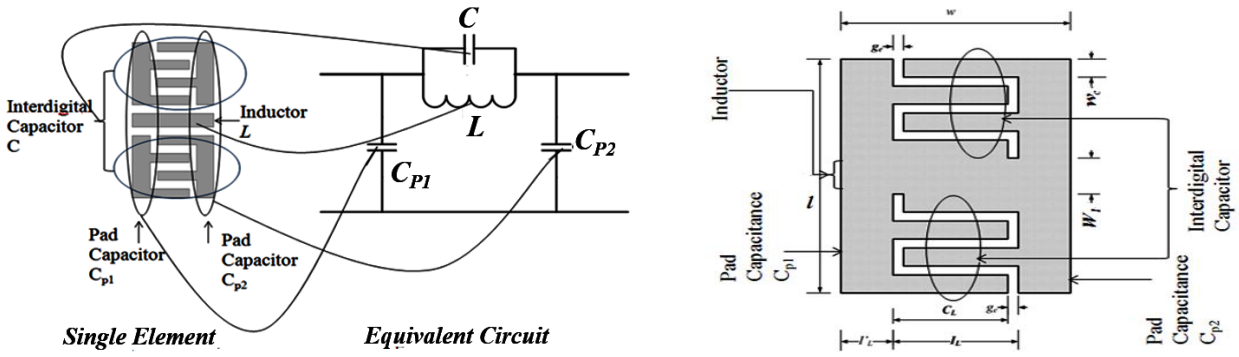

Figure 1. Quasi-lumped element resonator. (a) Subcomponent, (b) dimensioned.

capacitance of parallel conducting fingers on a substrate, and uses the capacitance that occurs across a narrow gap thin-film conductors. These gaps are essentially very long but folded to use a small amount of area, therefore compact area is obtained. In order to achieve maximum capacitance density, the finger width (w_1) must be approximately equal to inter-finger space (g_e). Also, the substrate thickness (h) should be much larger than the finger width. The capacitance can be increased by increasing the number of fingers, using a thin layer of high dielectric material between the substrate and conductor, or using an overlay high-k [5].

In this work a moderate dielectric constant was used and the equation to determine the IDC of the resonator was stated by Avenhaus in [6] and also appropriately stated in Eq. (2) of [7] for the same design specifications and considerations, where N is the number of fingers, C_L is the overlap length of IDC fingers, and $\Delta = 0.5(w_{eff} - w_1)$ (which is equal to 0.5 for this design) is the correction factor due to the effect of fringing field. The Q-factor of an inductor depends directly on the inductance, whereas the inductor is a single narrow straight inductor shorted across the IDC as shown in Figure 1(a). Normally, when inductor is narrow, it becomes more inductive but carry less current. As such, the inductance of a narrow strip inductor is decreased by the presence of a ground plane. Hence, an inductor width of 1.2 mm can comfortably carry sufficient current, while the entire structure of length 5.8 mm is broad enough to neutralize the effect of the presence of ground plane. The inductance of the structure is dominated by the magnetic field close to the centre strip and the value is dependent on the total length, spacing, and line width. The inductance L produced by the straight inductor can be calculated by Eq. (2) as stated in [8–13], and more specifically in Eq. (1) of [7] where I_L is the inductor length, W_1 is the inductor width, and t is the metal thickness as shown in Figure 1(b).

The IDC capacitor C and the inductor L are approximately calculated on the basis of $g_e/h < 1$ where g_e is the inter finger spacing, and h is the substrate thickness. It is evident from finite integration technique (FIT) analysis that the magnetic field lines do not loop around each finger but rather loop around the entire cross section of the interdigital width. Thus, the structure can be treated using microstrip transmission line theory, with ℓ as the length of the structure. The resonant frequency of the resonator is given in [12], also stated as Eq. (7) of [7] and it's dependent on, the inductor strip L, the capacitive inductance from the IDC (the length of the finger, the line width of the finger), and the pad capacitances, C_p where C is the IDC defined by Eq. (2) of [7], and L is the strip inductance defined by Eq. (1) of [7]. $C_{p1} = C_{p2}$ are pad capacitances defined by Eq. (6) of [7], and are formed between the gaps and the ground. The equation to determine the pad capacitance is also stated similarly in [13] where ℓ is the resonator length, and h is the substrate thickness. It is noteworthy that the pad capacitances do not depend on the size and the number of fingers, but rather on the substrate thickness, the length of the IDC, and finally, the effective line width. Therefore, it is also not impossible to have a large value of IDC without increasing the pad effect [14]. Essentially, the pads connected at both ends of the IDC acts as capacitor to ground with the sole aim of adjusting (tuning) the resonant frequency of the resonator, w_{eff} is the effective line width given in Eq. (2) [15] and ε_{eff} is the effective dielectric constant defined in Eq. (1).

$$\varepsilon_{eff} = \frac{(\varepsilon_r + 1)}{2} + \frac{(\varepsilon_r - 1)}{2}\left[1 + \frac{10h}{w}\right]^{-0.5} \tag{1}$$

$$w_{eff} = w + \frac{t}{\pi}\ln\left\{\frac{10.872}{\sqrt{\left(\frac{t}{h}\right)^2\left[\frac{1}{\pi\left(\frac{w}{t} + 1.10\right)}\right]^2}}\right\} \tag{2}$$

2.2. Problem Formulation of the Array

A planar array comprises definitely arranged finite sized identical antenna radiators which are fed by an appropriate feed network. In a way, the fields radiated from one radiator is received by the other

radiators. Hence, the signal get reflected, re-radiated, or scattered. The properties of these signals depends on the power of the signal, reflection coefficients, and possibly an additional electrical phase introduced due to propagation delay from one element to the other. This kind of interaction between the antenna elements and hence, can alter the array characteristics. Assume therefore that a planar array has $m \times n$ elements and are arranged in the xy-plane. In the x-direction, the number of array elements is $m = 9$, and in the y-direction the number of array is $n = 10$. If all the elements are fully excited by the proposed feed network, the pattern of the proposed array can be expressed as the product of the excited (actives) element factors and the array factor, in an analogous fashion to traditional array theory. To achieve this, it is assumed that 1) the element factor, $f(\theta)$ is identical to the pattern of a single element taken in isolation from the array, and is the same for any element in the array; 2) the overall pattern $\Sigma f(\theta)$ obtained is called the active patterns of the array; and finally, 3) $f(\theta)$ will depend on the position of the feed elements in the array such that edge elements will have active element patterns than the elements near the centre of the array, and for large array however, most of the elements will see a uniform neighbouring environment, and eventually, $f(\theta)$ can be approximated as equal for all elements in the array.

2.3. The Coupling Excitation

To achieve the conditions set in Section 2.2, the proposed array is fed by a feed probe network consisting of four coaxial probes located at the coordinates $p_1(x_s, y_s)$, $p_2(x_s, y_s)$, $p_3(x_s, y_s)$ and $p_4(x_s, y_s)$ to form two dimensional 2×2 source distribution as shown in Figure 1(a). The entire array elements were excited due to proximity coupling from the adjacent elements as a result of these four excitation coaxial probes to produce efficient excitation distribution. The antenna array lattice is arranged with four rectangular array lattices of 5×5 each (with the fifth column doubly overlapped to form the fifth column in each of the four lattices) and each is excited by a probe. The nodes of the array lattice are arranged in horizontal rows and vertical columns of similar inter element spacing of $\lambda_g/2$, where λ_g is the guided wavelength. The effective spacing between adjacent nodes in each column (d_y) is $0.159\lambda_{5.8\,\mathrm{GHz}}$ whereas that of horizontal (d_x) is $0.162\lambda_{5.8\,\mathrm{GHz}}$ as shown in Figure 2(b). Let the planar array antenna be arranged in a plane $z = 0$ as shown in the Figure 2(a), which consists of xy-plane and the xz-plane cross sections of the proposed rectangular planar antenna. Also, let the beam direction be determined by the coordinates of the nodes in a periodic Cartesian in the plane of direction *cosines* $x = \sin\theta \sin\phi$ and $y = \sin\theta \cos\phi$, where θ and ϕ are the angles measured at the axes z and x respectively. The excited elements ($p(x_s, y_s)$) in the figure with above coordinates are referred to as line sources (otherwise known as active elements or drivers). Consider the fact that a periodic lattice forms ($m \times n$) nodes in the xy-plane of the Cartesian

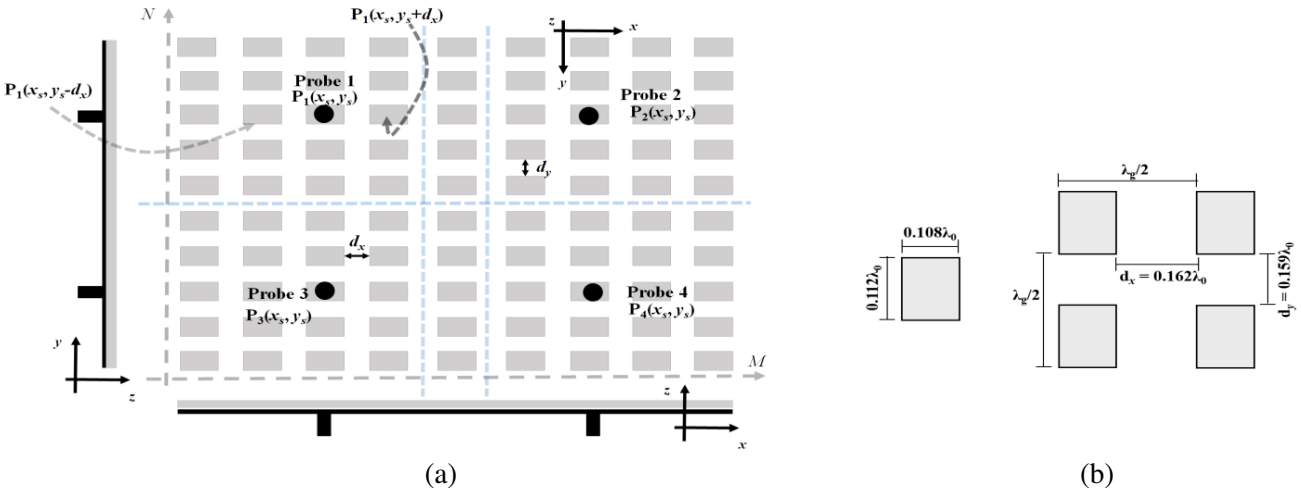

Figure 2. The array configuration. (a) The feed network, (b) the spacing.

coordinates with the polar radius of

$$R = \left[(md_x)^2 + (nd_y)^2\right]^{0.5} \tag{3}$$

from the centre of each $p(x_s, y_s)$ element. The periods of each lattice are d_x and d_y, as demonstrated in Figure 2(b). The positions of the nodes are denoted by $p = (m, n)$ and these nodes corresponds to the possible positions of the quasi-lumped element resonators where the black-undesignated elements of Figure 2(a) represent the passive elements. The nodes are excited by the coaxial feed probe network of four feeds, and consequently create radiation excitation patterns shown in Figure 3(a). The excitation of one of the elements of the array at each of the four lattices produces fringing field patterns that contribute to capacitance entries with the given array. These fringing fields also caused current to be induced in other nodes (passive elements) that in turn became active elements. Each radiating element is loaded with a via as shown in Figure 3(b) thus creating additional parallel inductance L. The inductance results from the current flowing through the vias, whereas capacitances C is simultaneously created due to the gap effect between the adjacent radiating elements. The combination of the inductance L and capacitance C forms the resonant tank LC. Equations to determine the values of the inductor L as well as the capacitor C are stated in Eq. (4) [16]. The advantage of this technique firstly, is that both the feed and the radiating elements lies on the surface of the substrate. As such, the otherwise pronounced surface waves are suppressed resulting in the provision of right impedance match between the radiating elements and the feeds. It also improves the antenna gain, and reduces back radiation.

$$L = \mu_0 h, \quad C = \frac{w\varepsilon_0\left(1+\varepsilon_r\right)}{\pi}\cosh^{-1}\left(\frac{2w+d_x}{d_x}\right) \tag{4}$$

Seeing that the antenna radiation pattern depends on the impedance at the antenna elements, the variation in the self- and mutual impedances due to the presence of coupling between the array elements for an array of $N \times M$ elements is as stated in Eq. (5) based on Figure 3(c) [17]. These impedance

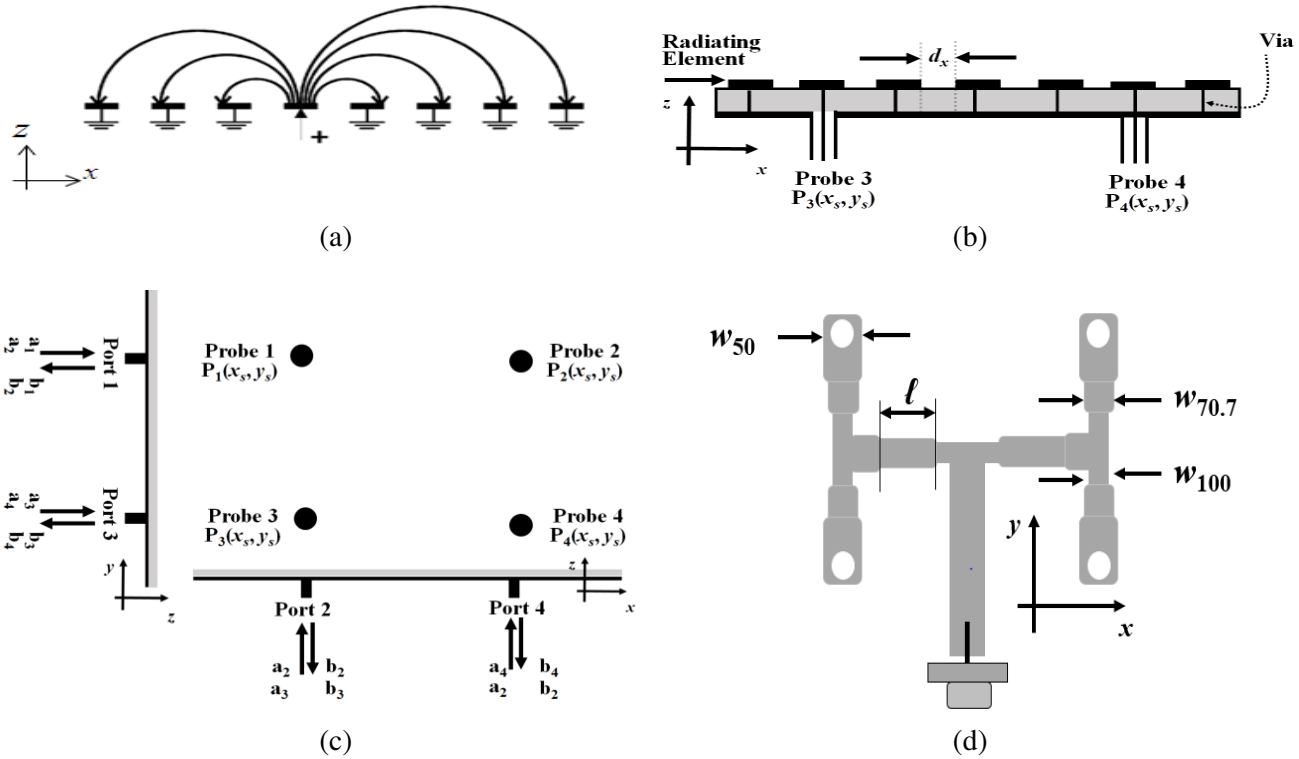

Figure 3. Radiation excitation pattern. (a) Excitation mechanism of one probe [18], (b) geometry showing the vias loading, (c) geometry of the four feed probes w.r.t S-parameters, (d) the in-phase feed network.

matrices of the excited self- and mutual impedances are dependent on 1) the type, and 2) configuration of the array. The mutual coupling of the four probes with respect to the incident waves and reflection coefficients are stated in matrix of Eq. (6) where a_1, a_2, ..., a_3 and b_1, b_2, ..., b_4 are the normalized excitation voltage waves. The respective currents and voltages as a results of the coaxial feed probes are stated in Eq. (7)

$$
\begin{aligned}
Z_{\text{Port1}} &= \begin{bmatrix} Z_{11}+Z_L & Z_{12} & Z_{13.....} & Z_{15} \\ Z_{21} & Z_{22}+Z_L & Z_{23....} & Z_{25} \\ . & . & . & . \\ Z_{51} & Z_{52} & Z_{53....} & Z_{55}+Z_L \end{bmatrix} \\
Z_{\text{Port2}} &= \begin{bmatrix} Z_{65}+Z_L & Z_{66} & Z_{67.....} & Z_{69} \\ Z_{75} & Z_{76}+Z_L & Z_{77....} & Z_{79} \\ . & . & . & . \\ Z_{105} & Z_{106} & Z_{107....} & Z_{109}+Z_L \end{bmatrix} \\
Z_{\text{Port3}} &= \begin{bmatrix} Z_{61}+Z_L & Z_{62} & Z_{63.....} & Z_{65} \\ Z_{71} & Z_{72}+Z_L & Z_{73....} & Z_{75} \\ . & . & . & . \\ Z_{101} & Z_{102} & Z_{103....} & Z_{105}+Z_L \end{bmatrix} \\
Z_{\text{Port4}} &= \begin{bmatrix} Z_{65}+Z_L & Z_{66} & Z_{67.....} & Z_{69} \\ Z_{75} & Z_{76}+Z_L & Z_{77....} & Z_{79} \\ . & . & . & . \\ Z_{105} & Z_{106} & Z_{107....} & Z_{109}+Z_L \end{bmatrix} \\
Z_T &= \begin{bmatrix} Z_{\text{Point1}} & Z_{\text{Point2}} \\ Z_{\text{Point3}} & Z_{\text{Point4}} \end{bmatrix}
\end{aligned} \tag{5}
$$

$$
\begin{aligned}
\begin{bmatrix} b_1 \\ b_2 \end{bmatrix} &= \begin{bmatrix} S_{11} & S_{12} \\ S_{21} & S_{22} \end{bmatrix} \begin{bmatrix} a_1 \\ a_2 \end{bmatrix}, \quad \begin{bmatrix} b_3 \\ b_4 \end{bmatrix} = \begin{bmatrix} S_{13} & S_{14} \\ S_{23} & S_{24} \end{bmatrix} \begin{bmatrix} a_3 \\ a_4 \end{bmatrix} \\
\begin{bmatrix} b_1 \\ b_3 \end{bmatrix} &= \begin{bmatrix} S_{31} & S_{32} \\ S_{41} & S_{42} \end{bmatrix} \begin{bmatrix} a_1 \\ a_3 \end{bmatrix}, \quad \begin{bmatrix} b_2 \\ b_4 \end{bmatrix} = \begin{bmatrix} S_{33} & S_{34} \\ S_{43} & S_{44} \end{bmatrix} \begin{bmatrix} a_2 \\ a_4 \end{bmatrix} \\
\begin{bmatrix} b_1 \\ b_2 \\ b_3 \\ b_4 \end{bmatrix} &= \begin{bmatrix} S_{11} & S_{12} & S_{13} & S_{14} \\ S_{21} & S_{22} & S_{23} & S_{24} \\ S_{31} & S_{32} & S_{33} & S_{34} \\ S_{41} & S_{42} & S_{43} & S_{44} \end{bmatrix} \begin{bmatrix} a_1 \\ a_2 \\ a_3 \\ a_4 \end{bmatrix}
\end{aligned} \tag{6}
$$

$$
\begin{aligned}
v_1 &= (Z_{\text{Port1}})^{0.5}(a_1+b_1), \quad v_2 = (Z_{\text{Port2}})^{0.5}(a_2+b_2), \\
v_3 &= (Z_{\text{Port3}})^{0.5}(a_3+b_3), \quad v_4 = (Z_{\text{Port4}})^{0.5}(a_4+b_4) \\
I_1 &= \frac{1}{(Z_{\text{Port1}})^{0.5}}(a_1-b_1), \quad I_2 = \frac{1}{(Z_{\text{Port2}})^{0.5}}(a_2-b_2), \\
I_3 &= \frac{1}{(Z_{\text{Port3}})^{0.5}}(a_3-b_3), \quad I_4 = \frac{1}{(Z_{\text{Port4}})^{0.5}}(a_4-b_4)
\end{aligned} \tag{7}
$$

From Eq. (7), $I_S = [I_1\ I_2\ I_3\ I_4]$ where I_S is the current in the active (source) nodes. For the N-element array, it is expected that the radiating elements can be characterized by these radiation modes as a result of the excitation from the active elements, in particular, the radiation characteristics of the proposed antenna as demonstrated in Figure 5. Therefore, the currents in the active nodes due to excitation of the probes is [19]

$$
I_s(z=0) = I(i,j) = \begin{cases} I_0, & \text{for } j=0 \\ \dfrac{I_0}{2n}, & \text{Otherwise} \end{cases} \tag{8}
$$

Equation (8) explicitly defined the current in the proposed active resonators where (i, j) represent current distributions along the horizontal and vertical cross section of each radiating element, whose values is I_0 at $j=0$ indicating that the values of currents in the shorted inductors of inductance L. The

feed network shown in Figure 3(d) is employed to provide in-phase excitations of the four active sources through the coaxial feed probes in order to forestall the occurrence of main beam steering seeing that phased array is not our objective. From this point of view of harmonic time dependence, the current in each of the active element formerly stated in Eq. (8) can be re-written as given in Eq. (9) below, where k_z is the z-direction propagation constant of the wave along the coaxial feed probes aperture (by which the active elements are excited) with its arbitrary value chosen in order to obtain the radiation characteristics of the radiating sources by spatial Fourier transform in the subsequent section.

$$I_s(z) = I_s(z=0)e^{(-jk)z} \tag{9}$$

Since the current is along the z-direction via the coaxial feed probes, the electromagnetic problem becomes a scalar one. The induced currents at various radiating elements will have different values for different radiating elements, but on the average, the induced currents in the radiating elements are expected to have the same excitation patterns as shown in Figure 3(a). The current $I_{\text{ind}}(k_z;\, z)$ at an arbitrary p^{th} radiator is induced by the local fields E_s^{loc} and thus have the relation stated in Eq. (10). The local field is the field produced by the excitation currents and the induced currents at all the radiating nodes except the $p(x_s, y_s)$ elements itself.

$$E_s^{loc} = \frac{1}{\alpha_s(k_z)} I_{\text{ind}}(z=0) \tag{10}$$

where

$$\alpha_s(k_z) = \frac{4}{\gamma(k_z)H_0^{(2)}(k_r d/2)}[20] \tag{11}$$

$$\gamma(k_z) = \frac{k_r}{k}\left(\frac{\mu_0}{\varepsilon_0}\right)^{0.5}, \quad k_r = \left(k^2 - k_z^2\right)^{0.5}, \quad \text{and} \quad k = \omega(\varepsilon_0\mu_0)^{0.5} \tag{12}$$

σ is the electrical conductivity of the elements, $H_0^{(2)}$ the Hankel function of the second kind and d the diagonal of each element.

2.4. The Radiation Pattern

Assume all of the currents are along the z-direction, and that, the electric field is polarized along the z-direction. Thus, electromagnetic propagation problem assumes a scalar dimension as earlier said. The active elements are located at point $p(x_s, y_s) = [p_1(x_s, y_s), p_2(x_s, y_s), p_3(x_s, y_s), p_4(x_s, y_s)]$ to create sufficient excitation density distributions, and the nearest neighbouring passive elements ($p^{'th}$) is at the point $p(x_s, y_s - g) = [p_1(x_s, y_s - g),\ p_2(x_s, y_s - g),\ p_3(x_s, y_s - g),\ p_4(x_s, y_s g)]$. The effective electric field acting on the nearest passive elements under consideration is the addition of the field produced by the active elements and that of the passive nodes. Therefore, this generated electric field creates interactions between the active elements and the surface of these nearest passive elements located at $p(x_s, y_s - g)$. The electric field generated by the active elements (sources) already reported in [19, 20] is

$$E^{\text{active-element}}(P(x,y), z=0) = -\frac{\gamma}{4}\left[\sum_{P(m,n)} I_{\text{ind}}(k_z;\, z=0)H_0^{(2)}(k_r|R|) + \sum_{P(x_s,y_s)} I_s(0)H_0^{(2)}(k_r|R|)\right] \tag{13}$$

where

$$|R| = |R_s - R_{s'}| \tag{14}$$

is the distance between the $p^{th}(m,n)$ and $p^{'th}(m,n)$ nodes on the same xy-plane, i.e.,

$$|R_s - R_{s'}| = \left[(m-m')^2 d_x^2 + (n-n')^2 d_y^2\right]^{0.5} \tag{15}$$

$$p^{'th}\text{ node} = \begin{cases} p_s(x_s, y_s - g), & \text{for } I_s(z) = 0 \\ p_s(x_s, y_s), & I_s \text{ as given in Eq. (4)} \end{cases} \tag{16}$$

The overall possible $p'(m,n)$ nodes except the source elements $p(x_s, y_s)$ gives the local field

$$E_s^{loc} = \sum_{p'(m,n)\neq p(x_s,y_s)} E_{p'(m,y)th-\text{node}} \tag{17}$$

Note that when $p(x_s, y_s)$ is very close to $p(x_s, y_s - g)$, the induced currents in other passive elements are quite small compared to the source element $p(x_s, y_s)$. Therefore, the main contribution to the local field at the surface of $p(x_s, y_s - g)$ element is the field radiated by each of the element source. Henceforth,

$$E_s^{loc} \approx E_s\left(x_s, y_s - g, z = 0\right) \tag{18}$$

Substituting Eq. (11) into Eq. (10), and using Eq. (13), this system of linear equations are obtained for the induced currents $I_{\text{ind}}(m, n)$ as

$$\sum_{p(m,n)p(x_s,y_s)} k_{p(m,n)p(x_s,y_s-h)} I_{\text{ind}}(m,n)(k_z; z=0) = \frac{1}{4}\alpha_s(k_z)\gamma \sum_{p(x_s,y_s)} H_0^{(2)}(k_r|R_s|) I_s(0) \tag{19}$$

where

$$k_{p(m,n)p(x_s,y_s-h)} = \delta_{p(m,n)p(x_s,y_s-h)} + \alpha_{p(m,n)}\gamma(k_z) H_0^{(2)}(k_r|R|)/4 \tag{20}$$

$\delta_{i,j}$ is the Kronecker delta function. Subsequently, the field at arbitrary point $P(x, y)$ produced by the whole structure can be calculated as shown in Eq. (21) below having obtained the induced currents $I_{\text{ind}}(k_z; z = 0)$ by solving the above system of linear equations.

$$E^{\text{active-element}}\left(P(x,y), z=0\right) = -\frac{\gamma}{4}\left[\sum_{P(m,n)} I_{\text{ind}}(k_z;\, z=0) H_0^{(2)}(k_r|R|) + \sum_{P(x_s,y_s)} I_s(0) H_0^{(2)}(k_r|R|)\right] \tag{21}$$

Consider a quasi-lumped resonator sources which has the following current distributions

$$I_S = I_S(0) J(z) \tag{22}$$

Therefore, the current distributions can be stated as

$$J(z) = \int_{-\infty}^{\infty} G(k_z) e^{jk_z z} dk_z \tag{23}$$

Hence, $G(k_z)$ can be determined as stated in Eq. (24) by performing the inverse Fourier transform of Eq. (23)

$$G(k_z) = \int_{-\infty}^{\infty} J_z(z) e^{-jkz} dk_z \tag{24}$$

where $G(k_z)$ is the Fourier transform of the current distribution function of the radiating element sources located at point $p(x_s, y_s)$. It is then apparent that the z-component of the electric field at any arbitrary point $p(x, y, z)$ generated by these sources can be determined by Fourier transform with respect to the parameter k_z seeing the solution for a radiating source problem gives the solution for the Fourier spatial harmonic of the antenna current. Hence, the linearity of the problem allow the use of the principle of superposition and as such, the electric field at any arbitrary point $p(x, y, z)$ produced by the sources is given as

$$E_z(x,y,z) = \int_{-\infty}^{\infty} G(k_z) E^{\text{Active-element}}\left(R, z=0\right) e^{-jkz} dk_z \tag{25}$$

where $E^{\text{Active-element}}(R, z = 0)$ is the electric field produced by each of the active element source $I_S(0)e^{jk_z z}$ stated in Eq. (21). The said radiating active element source exhibit the current distribution

$$J_z(z) = \sum_{i=1}^{N} \left[J_x(x,y) + J_y(x,y)\right] \tag{26}$$

where i is the i-th finger of each of the proposed radiating element; $J_x(x', y')$ & $J_y(x', y')$ are as stated in Eqs. (26) and (27); N is the number of fingers in the quasi-lumped radiator.

$$J_x(x', y') = \frac{\cos\left(\frac{2\pi}{w_c}x'\right)}{\pi w_c\sqrt{1-\left(\frac{2x'}{w_c}\right)^2}} \quad n = 0, 2, 4, 6, \ldots, 2n$$
$$\frac{\sin\left(\frac{2\pi}{w_c}x'\right)}{\pi w_c\sqrt{1-\left(\frac{2x'}{w_c}\right)^2}} \quad n = 1, 5, 7, 9, \ldots, 2(2n+1) \tag{27}$$

$$J_y(x', y') = \frac{\cos\left(\frac{2\pi}{w_c}y'\right)}{\pi w\sqrt{1-\left(\frac{2y'}{w}\right)^2}} \quad n = 0, 2, 4, 6, \ldots, 2n$$
$$\frac{\sin\left(\frac{2\pi}{w_c}y'\right)}{\pi w\sqrt{1-\left(\frac{2y'}{w}\right)^2}} \quad n = 1, 3, 5, 7, \ldots, 2(2n+1) \tag{28}$$

Using Eq. (24) as defined by [20], the electric far field can be express as

$$E^{\text{Far}} = \frac{E_z^{\text{array}}}{\sin\theta} \tag{29}$$

$$E^{\text{Far-field}}(r,\theta,\varphi) = \frac{jk_0G(k_z)e^{-jkr}}{2\pi r} \times \left[\sum_p I_pG(k_z)e^{jkr(x_p\cos\theta+y_p\sin\varphi)\sin\theta} + \sum_s I_sG(k_z)e^{jkr(x_s\cos\theta+y_s\sin\varphi)\sin\theta}\right] \tag{30}$$

$$E^{\text{Far-field}}(r,\theta,\varphi) = \frac{jk_0G(k_z)e^{-jkr}}{2\pi r} \times 2\sum_{p(x,y)} I_pG(k_z)e^{jkr(x\cos\theta+y\sin\varphi)\sin\theta} \tag{31}$$

Assume

$$f(x,y) = (\theta,\varphi) = I_{p(x,y)}G(k_z) \tag{32}$$

where $f_{(x,y)}(\theta,\phi)$ is the vector element radiation pattern. Hence, the far field radiation pattern can be further simplified as

$$E^{\text{Far-field}}(r,\theta,\varphi) = \frac{jk_0G(k_z)e^{-jkr}}{2\pi r}f_{(x,y)}(\theta,\varphi) \times 2\sum_{p(x,y)} e^{jkr(x\cos\theta+y\sin\varphi)\sin\theta} \tag{33}$$

$$E^{\text{Far-field}}(r,\theta,\varphi) = EP \times AF \tag{34}$$

It can subsequently be simplified as shown in Eq. (34) where EP is the radiation intensity of the element, and AR is the array factor.

$$EP = \frac{jk_0G(k_z)e^{-jkr}}{2\pi r}f_{(x,y)}(\theta,\varphi) \tag{35}$$

$$AF = 2\sum_{p(x,y)} e^{jkr(x\cos\theta+y\sin\varphi)\sin\theta} \tag{36}$$

where $x' = md_x$, $y' = nd_y$, $z' = 0$, $k = 2\pi/\lambda$, $x = x' \sin\theta\cos\phi$, and $y = y' \sin\theta\cos\phi$. Therefore, Eq. (34) represents the radiation pattern of the proposed array in 3-D. Hence, the radiation pattern of an array of $N \times M$-identical elements evaluated at location (θ, ϕ) in the far-field can be approximated by the product of radiation intensity of the element (EP) and the array factor (AR).

3. VALIDATION AND DESIGN SPECIFICATIONS

To explore the present explicit method numerically, the antenna was designed for 5.8 GHz to cover IEEE 802.11a WLAN U-NII Upper band based on the above-derived equations. The single element was first designed to confirm the performance of the proposed radiator first and foremost, as antenna candidate, and secondly, as a radiator with compact size capability and good directional characteristics. Subsequently, the planar array configuration was designed. The antenna was designed using 3D EM CST microwave studio, and printed on a grounded Roger Duroid RO4003C microwave substrate of 0.813 mm thickness (h) and relative permittivity of 3.38 with a metal thickness (t) of 0.035 mm. The antenna was excited by four coaxial feed probes network based on the principle of Wilkinson power divider as shown in Figure 3(d). The four probes are then soldered to the microstrip feed line and fed by a 50 Ω connector. The entire feed network is photo etched on a plastic spacer made from polyamide material (similarly demonstrated in [21, 22]) and mounted on the bottom of the structure in order to separate the feed network from the ground plane as shown in Figure 8(c). The horizontal probes are separated by distance of $2\lambda_{5.8\,\mathrm{GHz}}$ apart whereas, the vertical by $5\lambda_{5.8\,\mathrm{GHz}}/2$ apart, where $\ell = 5\lambda_{5.8\,\mathrm{GHz}}/4$, $w_{50} = 1.9$ mm, $w_{70.7} = 1.05$ mm, and $w_{100} = 0.46$ mm as shown in the figure. The radiating element dimensions were obtained from Eqs. (3) to (5) of [7], and are stated as follows: $l = 5.8$ mm, $w = 5.6$ mm, $C_L = 3.05$, $g_e = 0.3$ mm, $W = 1.2$ mm, $w_1 = 0.35$, $N = 8$, and $I_L = 3.35$ mm. These values were then substituted into Eqs. (1), (2), and (6) to determine the values of the strip inductance, interdigital capacitance, and the pad capacitances. The values are thereafter substituted into Eq. (3) to eventually obtain the desired resonance frequency of the design. Parametric optimization was further done using EM solver to ensure that resonance occur at the design specification. Using the explicit formula stated as Eq. (33) numerically, Figure 4(a) shows the array geometry of the proposed rectangular planar antenna array. A similar one was also designed as shown in Figure 4(b) but with microstrip patch (instead of the proposed radiator) for the purpose of comparative analysis. In both, the numbers of nodes in the structure are 9×10. The supposedly active elements were positioned at the centre of each 5×5 sub-array lattice at coordinate of $p(x_s, y_s)$. The inter-element spacing of $\lambda_g/2$ was used on both axes where λ_g is the guided wavelength calculated to be 28 mm at a resonant frequency of 5.8 GHz, whereas the elements are periodic with periods d_x and d_y equal to $0.162\lambda_{5.8\,\mathrm{GHz}}$ and $0.159\lambda_{5.8\,\mathrm{GHz}}$ respectively at $\lambda_{5.8\,\mathrm{GHz}}$ which is equals 51.72 mm, where λ_0 is the free space wavelength at the antenna resonance

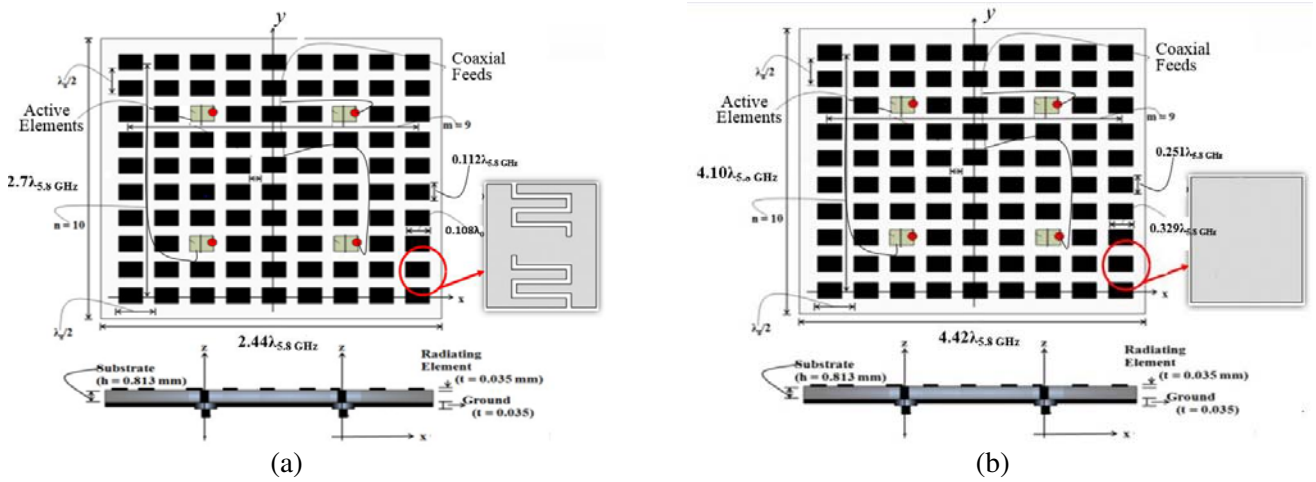

Figure 4. Geometry of the antenna array. (a) Proposed, (b) patch.

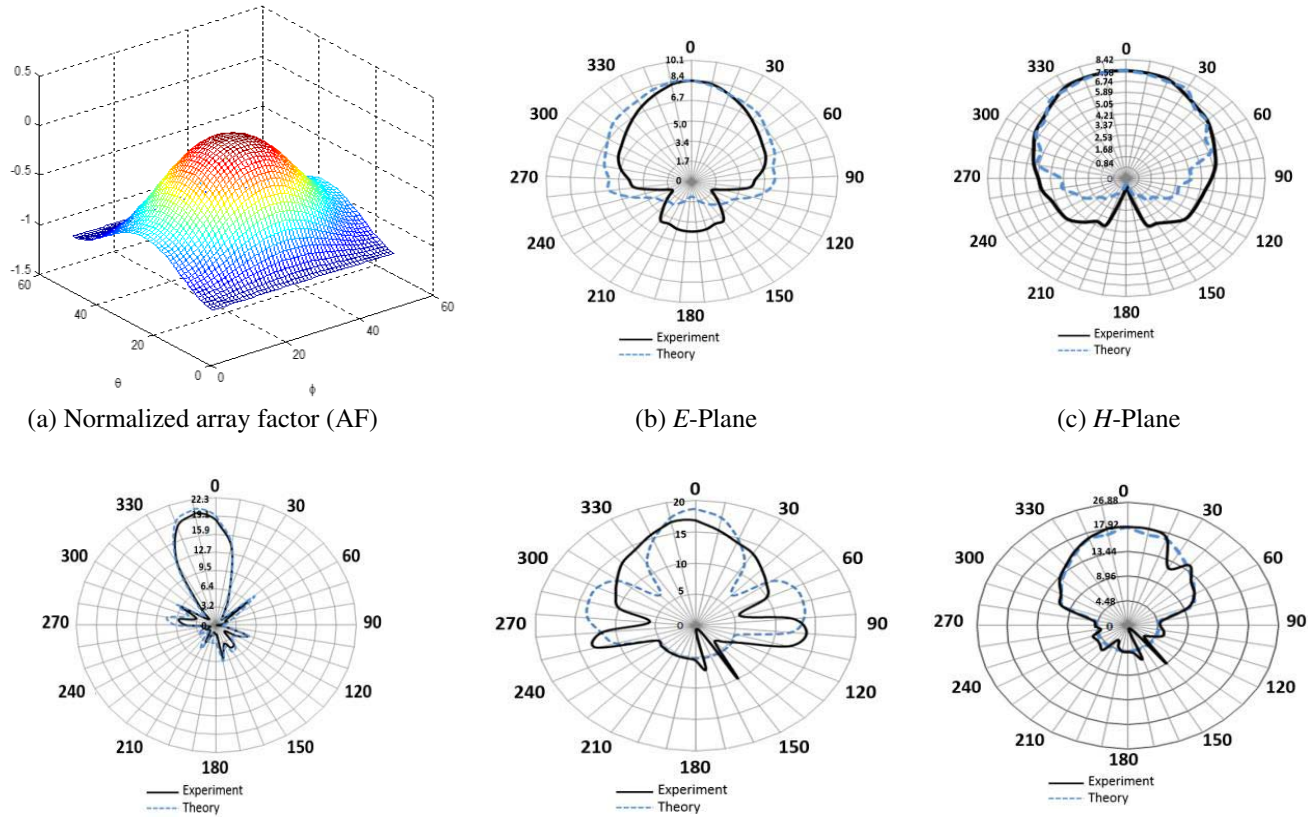

(a) Normalized array factor (AF) (b) *E*-Plane (c) *H*-Plane

(d) *E*-Plane (e) *H*-Plane (f) *E*-Plane of the patch array

Figure 5. Radiation pattern of the antenna. (a) Normalized array factor (AF), (b), (c) single element proposed antenna, (d), (e), (f) proposed planar array antenna.

frequency using Eq. (3). The radiation pattern at H-plane along broadside for such antenna systems was calculated at the resonance frequency. E-polarization was also determined using the explicit formula stated in Eq. (33). Subsequently, the design was simulated, fabricated and measured. The results were then compared with the numerical formula stated in the said explicit equation. Each radiating element of the proposed antenna and microstrip patch were 5.8×5.6 and $17 \times 13\,\text{mm}^2$ in dimensions respectively. The array factor (AF) of the proposed planar antenna array configuration was computed using Eq. (31) and the 3-D plot which is dependent on both $\theta = 90^\circ$ and $\varphi = 0$ where (m, n) equal 9 and 10 respectively is as shown in Figure 5(a). The design was also simulated and measured, and the radiation patterns both in E- and H-planes for both the single element and the array were presented. Figures 5(b) & (c) show the simulated and experimental radiation patterns of the proposed single element whereas Figures 5(d) & (e) depict that of the array configuration. For the simulation results of the single element, the main magnitude was 8.4 dB in a direction of zero degree with an angular width (HPBW) of 32.6 degree, and side lobe level of -6.13 dB. The measured values indicated that the main lobe magnitude was 7.6 dB, main lobe with spatial radiation of 5 degree away from the boresight with an angular width (HPBW) of 30.4 degree, and a side lobe level of -4.2 dB in xz-plane (E-plane). Similarly in yz-plane (H-plane), the simulation results show that the main lobe magnitude was 8.4 dB with a main lobe direction of zero degree at an angular width (HPBW) of 88.19 degree, whereas the measured results show that the main lobe magnitude was 7.6 dB, and a main lobe direction of 6 degree at an angular width (HPBW) of 87.4 degree. In Figure 5(d), the main lobe magnitude was 19 dB, the only major lobe was oriented along $\theta = 10$ degrees and the angular width (3 dB) is 13 degrees, whereas the side lobe level was less than -10.2 dB. In H-plane shown in Figure 5(e), the major lobe was oriented along $\theta = 8$ degrees with magnitude of 19 dB, angular width (at 3 dB) of 22 degrees and side lobe level of -4.3 dB. The reasons for these 5, 6, 10 and 8 degrees squint from the principal axis

as demonstrated in Figures 5(d)–(f) is as a result of spacing differential between the horizontal and vertical periods ($d_y - d_x$) which is equals to $0.159\lambda_{5.8\,\mathrm{GHz}} - 0.162\lambda_{5.8\,\mathrm{GHz}}$ of the array. Comparing the explicit numerical result with the simulation and experimental results demonstrates to a large extent, a reasonable degree of agreement, though with minor discrepancies particularly as shown in Figure 5(e). The reason for this dissimilarity is not unconnected with the inability to precisely locate the excitation feeds positions during fabrication with respect to the simulated feed positions. In both, one major main lobe is observed, whereas a side-lobe level of -10.2 dB is noticed in both the simulated and experimental results particularly in xz-plane. Figure 5(f) shows the E_θ component radiated by a rectangular array in the plane cut by $\varphi = 0$ of the microstrip patch antenna, where the major lobe is oriented along 5 degrees. The antenna beamwidth (HPBW) is 41 degrees with a side lobe level of -13.4 dB. However, a minor level of back lobe is formed in the lower part of the hemisphere which may be due to the existence of radiations from the surrounding objects. Generally, the radiation patterns of the antennas obtained are close to a directional type, and the beam width of the proposed antenna is 31.7% narrower than the patch antenna. The radiation pattern of the antenna is acceptable, and there is a good agreement between the theory and the measured results.

Comparing the radiation pattern of the proposed shown in Figure 4(a) with the patch antenna of Figure 4(b) shown in Figure 5 (and in particular Figures 5(c) & (d) indicates that the proposed E-plane radiation pattern exhibits a narrow beamwidth of about 13 degree compared to the 41 degree width exhibited by the patch with a beamwidth differential of about 28 degree. However, the patch antenna exhibited a lower sidelobe level differential of about 3 dB. The orientation of the major lobe of the E-plain pattern away from boresight as shown in Figure 5(d), as well as the major lobe E-plain squint was investigated to determine the cause. It was discovered that the vertical spacing d_y is $0.159\lambda_{5.8\,\mathrm{GHz}}$ (which is equal to 4.45 mm) whereas that of horizontal (d_x) is $0.162\lambda_{5.8\,\mathrm{GHz}}(= 4.54\,\mathrm{mm})$ as shown in the figure. The overall spacing distance of $\lambda/2$ is employed to ensure that the spacing is not greater than $\lambda/2$. If it does, multiple maximal of equal magnitude can be formed. To avoid grating lobes in x-z and y-z planes of rectangular array, the spacing between elements should in x and y-directions respectively must be less than $\lambda/2$. This is the very reason why the entire spacing is $\lambda/2$ whereas, the differential spacing on both directions are [d_y is $0.159\lambda_{5.8\,\mathrm{GHz}}$ & (d_x) is $0.162\lambda_{5.8\,\mathrm{GHz}}$].

Figure 6(a) demonstrates the simulated and experimental return loss results for a single quasi-lumped element resonator whereas Figure 6(b) shows the simulated and measured return loss results of the proposed array along its patch counterpart. In Figure 6(a), the experimental pattern bandwidth is 5.74–5.98 GHz and a gain of about 9.4 dBi using gain absolute method whereas its experimental input impedance is $51.071 - j1.09\,\Omega$. Also, the theoretical and experimental return loss results of the proposed and the microstrip patch planar antenna array were given in Figure 6(b). The figure shows that the experimental pattern bandwidth of the proposed antenna is 5.72–5.87 GHz with a gain of 19.79 dBi, whereas the experimental input impedance was $49.58 - j1.08$ with a VSWR of 1.081:1 which is around 50 Ohms with marginal reactive component of $1.09\,\Omega$ indicating good impedance match. This

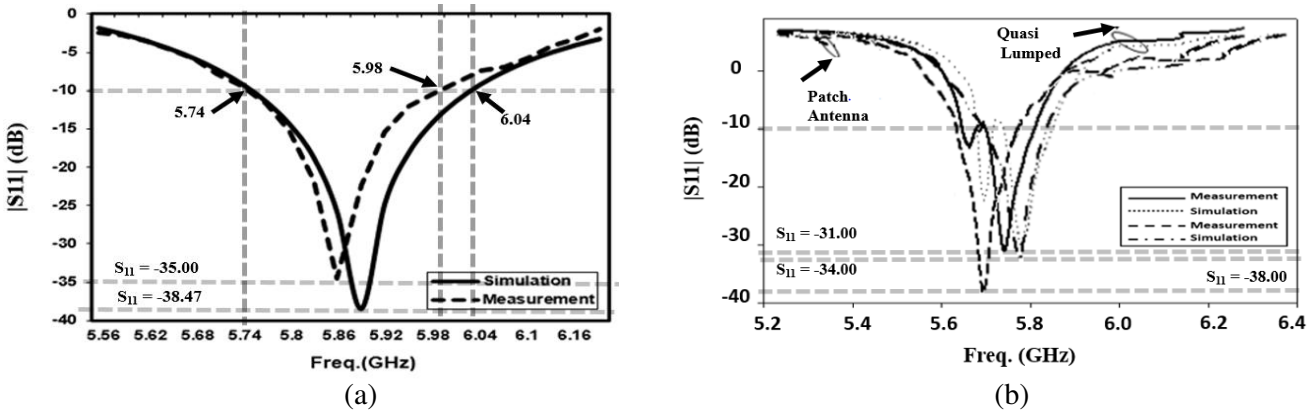

Figure 6. Theoretical and experimental return loss of the proposed. (a) Single element, (b) proposed and patch antenna array.

is supported by Figure 7 which shows the simulated and measured voltage standing wave ratio (VSWR) of the proposed and the patch array antennas.

The area occupied by the proposed antenna can be determined by Eqs. (37) and (38).

$$A(x,y) = \int_{x_i}^{m=9} \int_{y_i}^{n=10} A(x_i, y_i)(x,y)dxdy \tag{37}$$

$$A(x,y) = \sum_{x_i}^{m=9} \sum_{y_i}^{n=10} \left[(l_{y_i} + 0.159)\left(b_{x_i} + 0.162\right)\right] \tag{38}$$

where l_y and b_x are the length and breadth of the radiating elements respectively. Using Figure 2(a), the length and breadth of the proposed is determined by

$$l_y(x,y) = (0.112 + 0.159)\lambda_{5.8\,\mathrm{GHz}} \times 10 = 2.71\lambda_{5.8\,\mathrm{GHz}}$$

$$b_x(x,y) = (0.108 + 0.162)\lambda_{5.8\,\mathrm{GHz}} \times 9 = 2.43\lambda_{5.8\,\mathrm{GHz}}$$

and thus the area can be stated as $2.71\lambda_{5.8\,\mathrm{GHz}} \times 2.43\lambda_{5.8\,\mathrm{GHz}}$. Hence, the estate area of the patch can

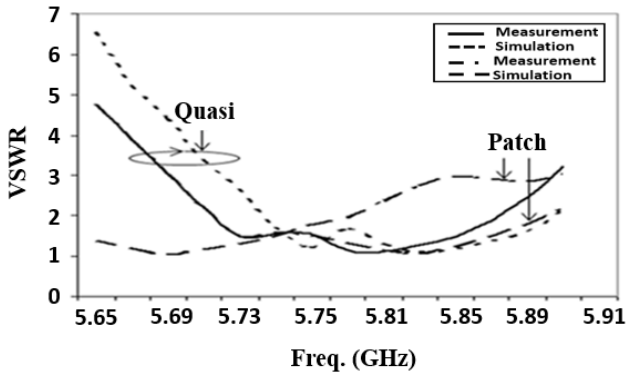

Figure 7. Theoretical and experimental voltage standing wave ratio.

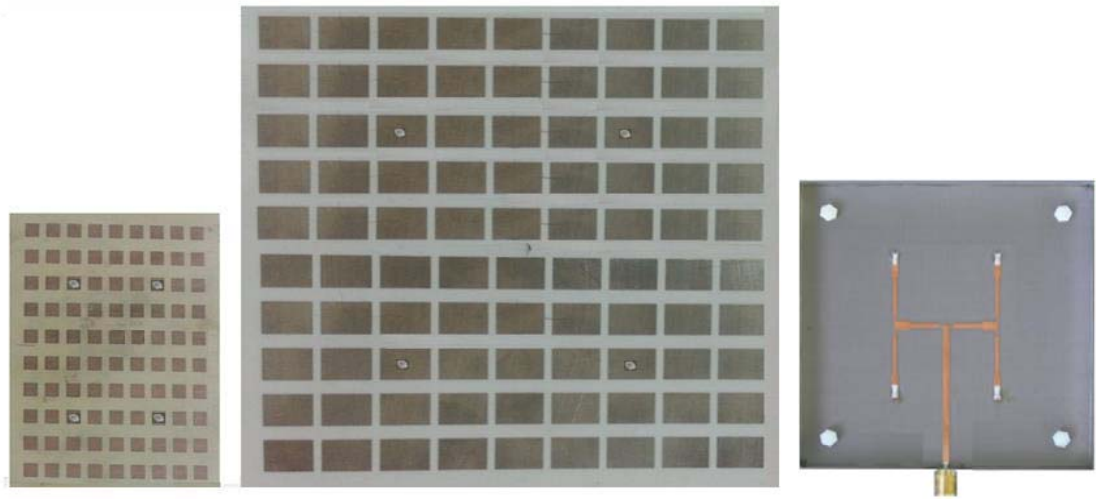

Figure 8. The capture of the fabricated antennas. (a) Proposed, (b) patch, (c) the coupling mechanism.

Table 1. Performance comparison of the proposed antenna.

Antenna Types	Sizes (sq. mm)	Resonance Freq. (GHz)	Measured Bandwidth (MHz)	Measured Gain (dBi)	
Quasi Lumped Element	$2.71\lambda_0 \times 2.43\lambda_0$	5.80	190	19.79	
Microstrip Patch	$4.1\lambda_0 \times 4.42\lambda_0$	5.80	100	17.92	
Antenna Types	Return Loss (dB)	Beamwidth (degree)	VSWR	Aperture Efficiency	Radiation Efficiency
Quasi Lumped Element	34.00	13	1.081:1	72.80	69.18
Microstrip Patch	38.00	41	1.044:1	65.80	65.56

subsequently be determined similarly.

$$l_y(x,y) = (0.251 + 0.159)\lambda_{5.8\,\mathrm{GHz}} \times 10 = 4.1\lambda_{5.8\,\mathrm{GHz}}$$
$$b_x(x,y) = (0.329 + 0.162)\lambda_{5.8\,\mathrm{GHz}} \times 9 = 4.42\lambda_{5.8\,\mathrm{GHz}}$$

Thus given estate area of $4.1\lambda_{5.8\,\mathrm{GHz}} \times 4.42\lambda_{5.8\,\mathrm{GHz}}$. Comparing the proposed area with the patch antenna as shown in Figure 8 therefore gives area reduction of about 63.86%.

Table 1 gives further performance profile comparison summary of the proposed antenna with respect to the patch antenna. It is conspicuous that the proposed antenna real estate is 57.42% better that the patch, with a bandwidth of 47.37%, a marginal gain of 10.44%, but with an inferior return loss of 23.6% and VSWR (shown in Figure 7) of 3.42%. With the inferior return loss and VSWR notwithstanding, both the return loss and VSWR of the proposed antenna were very significant.

4. CONCLUSION

An experimental design of a compact quasi-lumped element resonator planar antenna array with fixed beam has been presented. The proposed antenna array is fed by a coaxial feed probe network to provide even excitation distributions. It exhibits significant antenna real estate reduction of 74.74% over the microstrip patch antenna, better gain differential of 13% and a moderate side lobes level. These results are promising, and the architecture can easily be integrated with printed structures. In essence therefore, the volume of the proposed antenna is sizeable and as such becomes cost effective (as the antenna construction cost is proportional to antenna volume). Besides, the effective aperture size (notwithstanding its compact size) allows for optimal efficiency due to the associated capacitive and inductive contributions from the antenna elements.

REFERENCES

1. Janhsen, A., B. Schiek, and V. Hansen, "On the definition of quasi lumped elements in planar microwave circuits," *22nd European Microwave Conference*, Vol. 1, 251–256, Sep. 5–9, 1992,
2. Sarabandi, K. and R. Azadegan, "Design of an efficient miniaturized UHF planar antenna," *IEEE Transactions on Antennas and Propagation*, Vol. 51, No. 6, 1270–1276, 2003.
3. Abu-Abed, A. S. and R. G. Lindquist, "Capacitive interdigital sensor with inhomogeneous nematic liquid crystal film," *Progress In Electromagnetics Research B*, Vol. 7, 75–87, 2008.
4. Rosu, I., "Microstrip, strapline, and CPW design," YO3DAC/VA3IUL, http://www.qsl.net/va3iul, 2014.

5. Bahl, I., *Lumped Element for RF and Microwave Circuits*, Artech House, 2003.
6. Avenhaus, B., "Characterization of high temperature superconducting thin films and their microwave application," PhD Thesis, Faculty of Engineering, University of Birmingham, Sep. 1996.
7. Ain, M. F., S. S. Olokede, Y. M. Qasaymeh, A. Marzuki, J. J. Mohammed, S. Srimala, S. D. Hutagalung, Z. A. Ahmad, and M. Z. Abdulla, "A novel 5.8 GHz quasi-lumped element resonator antenna," *Int. J. Electron. Commun. (AEU)*, Vol. 67, 557–563, 2013.
8. Huang, F., B. Avenhaus, and M. J. Lancaster, "Lumped-element switchable superconducting filters," *IEE Proc. Microwave on Antennas Propag.*, Vol. 146, No. 3, 299–233, 1999.
9. Wadell, B. C., *Transmission Line Design Handbook*, Artech House, Boston, 1991.
10. Su, H. T., F. Huang, and M. J. Lancaster, "Compact pseudo-lumped element quasi-elliptic filters," *IEE Colloquium on Microwave Filters and Multiplexers*, No. 2000/117, Nov. 2000.
11. Bogatin, E., "Design rule for microstrip capacitance," *IEEE Trans. on Components, Hybrids and Manufacturing*, Vol. 11, 253–259, Sep. 1988.
12. Yin, X.-C., C.-L. Ruan, C.-Y. Ding, and J.-H. Chu, "A compact ultra-wideband microstrip antenna with multiple notches," *Progress In Electromagnetics Research*, Vol. 84, 321–332, 2008.
13. Hong, J.-S., *Microstrip Filters for RF/Microwave Applications*, Wiley Inter Sciences, John Wiley & Sons, Hoboken, N. J., Jan. 6, 2011.
14. Naghed, M. and I. Wolf, "Equivalent capacitances of coplanar waveguide discontinuities and interdigitated capacitors using a three-dimension finite difference method," *IEEE Trans. on Microwave Theory and Techniques*, Vol. 38, No. 12, 1808–1815, 1990.
15. Wheeler, H. A., "Transmission-line properties of a strip line between parallel planes," *IEEE Trans. on Microwave Theory and Techniques*, Vol. 26, No. 11, 866–876, 1978.
16. Gao, Y. X., K. M. Luk, and K. W. Leung, "Mutual coupling between rectangular dielectric resonator antenna by FDTD," *Proc. Inst. Elect. Eng.-Microwave Antennas Propagation*, Vol. 146, No. 4, 292–294, Aug. 1999.
17. Gupta, I. J. and A. A. Kseinski, "Effect of mutual coupling on the performance of adaptive arrays," *IEEE Transactions on Antennas and Propagation*, Vol. 31, No. 5, 785–791, 1983.
18. Mamishev, A. V., K. Sundara-Rajan, F. Yang, and Y. Du, "Interdigital sensors and transducers," *Proceedings of the IEEE*, Vol. 92, No. 5, 808–845, May 2004.
19. He, S., C. R. Simosvki, and M. Popov, "An explicit and efficient method for obtaining the radiation characteristics of wire antennas in metallic photonic band gap structures," *Microwave and Optical Tech. Letters*, Vol. 26, No. 2, 67–73, 2000.
20. Simosvki, C. R. and S. He, "Antennas based on modified metallic photonic band gap structures consisting of capacitively loaded wires," *Microwave and Optical Tech. Letters*, Vol. 31, No. 3, 214–221, 2001.
21. Drossos, G., Z. Wu, and L. E. Davis, "Four-element planar arrays employing probe-fed cylindrical dielectric resonator antennas," *Microwave and Optical Tech. Letters*, Vol. 18, No. 5, 315–319, Aug. 1998.
22. Bartyzal, J., T. Bostik, P. Kavacs, T. Mikulaseky, J. Puskely, Z. Randa, L. Slama, J. Vorek, and D. Wolansky, "Antenna arrays for tactical communication systems: A comparative study," *Radioengineering*, Vol. 20, No. 4, 817–827, Dec. 2011.